J Solid State Electrochem (2005) 9: 337–346
DOI 10.1007/s10008-004-0627-5

ORIGINAL PAPER

A. Seyeux · V. Maurice · L. H. Klein · P. Marcus

In situ scanning tunnelling microscopic study of the initial stages of growth and of the structure of the passive film on Ni(111) in 1 mM NaOH(aq)

Received: 7 September 2004 / Revised: 28 October 2004 / Accepted: 28 October 2004 / Published online: 14 April 2005

Abstract In situ electrochemical scanning tunnelling microscopic (STM) measurements of the growth mechanism of the passive film on Ni(111) single-crystal surfaces in an alkaline 1 mM NaOH aqueous solution are reported. Stepping the potential from −1,050 mV/SHE, where the terrace topography of the bare Ni(111) surface is observed, to −800 mV generates a continuous step flow resulting from a slow dissolution of the surface localized at step edges of the surface. Islands are observed on the terraces that possibly correspond to the specific adsorption of hydroxide anions, without formation of an ordered structure. The nucleation of the passivating oxide is preferentially located at the step edges at this potential. The ongoing dissolution at the nearby step edges not yet passivated leads to the formation of isolated 2D islands of the passivating oxide. At −780 mV, the formation of extended islands constituted of 2D nanocrystals (∼2 nm) is observed on the substrate terraces and blocks the dissolution at the step edges. The nanocrystals have an hexagonal lattice assigned to the formation of a monolayer of $Ni(OH)_2(0001)$ in strained epitaxy on Ni(111). At $E \geq -630$ mV, the formation of a facetted topography is observed as a result of the 3D growth of the passive film in tilted epitaxy on the substrate. Its structure is in excellent agreement with that expected for an unstrained 3D β-$Ni(OH)_2(0001)$ layer. This 3D layer of β-$Ni(OH)_2$ is not reduced by a cathodic sweep of the potential down to −1,500 mV whereas the 2D islands are reduced under similar conditions. Ageing of the passive film shifts cathodically the potential of non-reversibility.

Special issue for Prof. Gyorgy Horanyi on the occasion of his 70th birthday, in recognition of his outstanding contribution to Electrochemistry and Material Science.

A. Seyeux · V. Maurice (✉) · L. H. Klein · P. Marcus (✉)
Laboratoire de Physico-Chimie des Surfaces,
CNRS-ENSCP (UMR# 7045), Ecole Nationale
Supérieure de Chimie de Paris, 11 rue Pierre et Marie Curie,
75231 Paris Cedex 05, France
E-mail: philippe-marcus@enscp.jussieu.fr

Keywords Passivation · Structure · Growth mechanism · Nickel · Oxide · Hydroxide

Introduction

The polarization of nickel electrodes in alkaline aqueous electrolytes is characterized by anodic (A_1, A_2) and cathodic (C_1, C_2) peaks (see Fig. 1) that are related to the formation and reduction of anodic oxides grown on the surface [1–15]. The A_1 and A_2 anodic peaks are related to the oxidation of Ni^0 to Ni^{2+} and Ni^{2+} to Ni^{3+}, respectively. The C_1 and C_2 cathodic peaks correspond to the reduction of Ni^{3+} to Ni^{2+} and Ni^{2+} to Ni^0, respectively. In acidic solution, an intense A_1 peak is observed [2–4, 12]. It is associated with the fast dissolution reaction of the Ni surface that precedes the growth of the passive film. In alkaline solution [1, 5–11, 13, 14], dissolution is minimized as shown by detailed analysis of cyclic voltammetry measurements [11] and quartz crystal microbalance data [15]. The reducibility of the Ni^{2+} oxide film depends on potential. The protective layer can be reduced if the anodic potential of formation does not exceed the value of −0.4 to −0.5 V_{SHE}. This limit has been associated with the irreversible transformation of a reducible phase (assigned to α-$Ni(OH)_2$) into a nonreducible phase (assigned to β-$Ni(OH)_2$) [8–10, 16].

The Ni^{2+} passive film formed on nickel can be described by a bilayer model with the inner part consisting of nickel oxide (NiO) and the outer part of a hydroxylated NiO surface or a 3D nickel hydroxide ($Ni(OH)_2$) layer, possibly hydrated [8, 10, 17–32]. In acid solution, the thickness of the passive film has been measured to range between 0.9 nm and 1.2 nm [3, 4, 17–19, 22, 27], some authors reporting a small gradual increase up to 2 nm with increasing potential [25, 30–32]. In alkaline solution, it has been observed that the thickness of the outer hydroxide layer is larger than in acid solutions and remains constant (∼1.5 nm) in the Ni^{2+} passive range [25], whereas the thickness of the inner oxide layer,

forming the barrier layer against corrosion, increases linearly with potential up to 3 nm. Other authors conclude to a total thickness of the passive layer ranging from 1 nm to 2 nm [7, 8, 11, 20].

The structure of the passive film formed in acidic solution is well documented [12, 30–37]. It is crystalline with NiO growing along the (111) direction in antiparallel epitaxy. The (111) orientation is stabilized by surface hydroxylation. The surface of the inner NiO(111) crystalline structure is facetted as a result of a tilt of the oxide lattice with respect to the substrate lattice [12, 30–32, 35–37]. A noncrystalline structure has also been observed in situ [30–32, 34]. It has been assigned to a thicker and likely porous layer of hydrated hydroxide (possibly α-Ni(OH_2)) covering the inner NiO(111) crystalline structure [30, 31]. In alkaline solution, fewer results have been reported. A crystalline lattice of hexagonal symmetry has been observed on Ni(100) [38] and Ni(111) [16] that can correspond to the growth of NiO(111) or $Ni(OH)_2$(0001) (α or β). On Ni(100), an intermediate nonhexagonal structure has been observed prior to the formation of the NiO(111) or $Ni(OH)_2$(0001) hexagonal phase [38]. It was assigned to a strained 2D oxide or hydroxide layer formed in the initial stages of growth of the passive film on the Ni(100) surface.

The objective of the experiments reported here was to obtain detailed structural data on the growth mechanism of the passive film formed on Ni(111). In situ electrochemical scanning tunnelling microscopy (EC-STM) was used. An alkaline aqueous solution (1 mM NaOH(aq), pH 11) was selected in order to slow down the dissolution reaction that occurs in acidic solution, which modifies the surface topography in the initial stages of growth of the passive film. The structural changes occurring on the metallic nickel surface, from the initial stages of oxidation (onset of A_1 peak) to the later stages where 3D crystalline Ni^{2+} layers are formed, have been investigated.

Experimental

Ni(111) single-crystals oriented within $\pm 1°$ by Laüe back-diffraction were used. The surface was mechanically polished with diamond spray with a final grade of 0.25 μm. It was then electropolished in 55% sulfuric acid for 7 min at 0.3 A/cm^2 and subsequently annealed at 1,273 K for 16 h in a flow of ultra pure hydrogen (6 N) at atmospheric pressure to heal out the defects and to enlarge the terraces. The sample was then transferred in air to the electrochemical cell of the STM. The area exposed to the electrolyte was 0.16 cm^2. The EC-STM cell was made of Teflon and contained a Pt counter electrode and a Pt pseudoreference electrode. The reference electrode was calibrated by the well-defined peaks of the polarization curve of Ni in 1 mM NaOH(aq) (Fig. 1) and proved to be sufficiently stable. In the following, all potentials are given with respect to the standard hydrogen electrode (V/SHE). Prior to each measurement, the EC-STM cell with the two Pt electrodes mounted was cleaned first in a 2:1 mixture of concentrated H_2SO_4 and H_2O_2 and then in concentrated HNO_3 and finally thoroughly rinsed with Millipore water (resistivity >18 MΩ cm).

The measurements were performed in 1 mM NaOH(aq) solution prepared from ultrapure 5 M NaOH (Merck) and Millipore water. After a cathodic pretreatment in the electrolyte to reduce the air-formed oxide film, the electrode was stepped to the potential of interest. The reduction pre-treatment consisted of three cycles of potential between −500 mV and −1,500 mV. Care was taken not to overpass the potential of nonreversibility (−500 mV) during cycling.

The EC-STM instrument used was a molecular imaging system (PicoSPM with STM A head, PicoScan 2100 controller and PicoStat bi-potentiostat). The tungsten tips were prepared from a 0.3-mm diameter wire by electrochemical etching in 3 M NaOH(aq) and covered by Apiezon wax. All images were obtained in the topographic mode. The reported lattice parameter values have been averaged over ten measurements of distances extending over at least ten periods of the unit cell.

Results

Figure 1 shows two successive cyclic voltamograms of Ni(111) in 1 mM NaOH(aq) recorded in a classical electrochemical cell. The potential was cycled between the hydrogen and oxygen evolution regions, starting downwards from −500 mV. The anodic peaks A_1 and A_2 are related to the oxidation of Ni^0 to Ni^{2+} and of Ni^{2+} to Ni^{3+}, respectively. The cathodic peaks C_1 and C_2 correspond to the reduction of Ni^{3+} to Ni^{2+} and of Ni^{2+} to Ni^0, respectively. The first cathodic scan shows that the C_1 peak is observed when the applied potential has not exceeded −500 mV (it was also observed during the pretreatment when the potential was cycled between −500 mV and −1,500 mV). In contrast, the C_1 peak is not observed during the second cathodic scan. This indicates that a nonreducible Ni^{2+} oxide layer has been formed when the potential has been scanned above −500 mV during the first cycle. The presence of the non reducible Ni^{2+} oxide layer is confirmed by the absence of the A_1 anodic wave during the second anodic scan. These results on the effect of the applied potential on the reducibility of the Ni^{2+} oxide layer are in good agreement with previous observations [8, 9, 16, 38]. The STM measurements described below were performed at the characteristic potential of −1,150, −800, −780, −630 and −280 mV pointed by arrows in Fig.1.

The topography of the metallic Ni(111) surface has been systematically checked at −1,150 or −1,050 mV prior to the study of the modifications resulting from the polarization in the potential region of the A_1 peak. Figure 2 shows a typical image obtained at −1,150 mV.

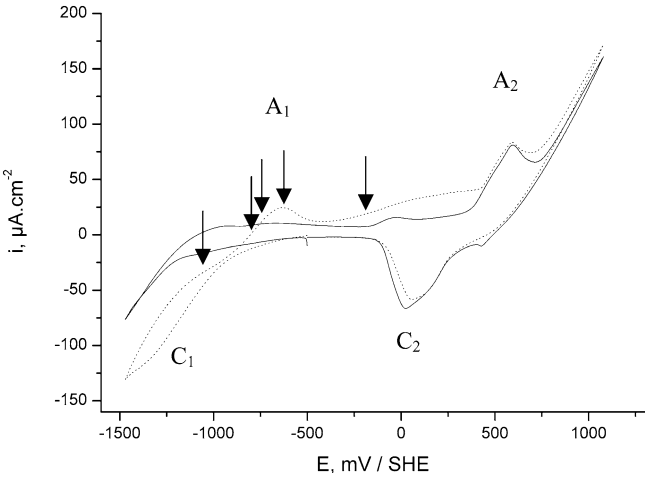

Fig. 1 Potentiodynamic polarization curves of Ni(111) recorded in 1 mM NaOH(aq) at a scan rate of 20 mV s^{-1}. The potential was cycled downwards from the starting value of −500 mV. The *dotted* and *solid lines* correspond to the first and second cycles, respectively. The A_1 and A_2, anodic peaks and C_1 and C_2 cathodic peaks are marked. The *arrows* point the characteristic potentials investigated by EC-STM

The terrace and step topography characteristic of the well-crystallized metallic surface is observed. The width of the terraces is ~20 nm. The measured step height is 0.2 ± 0.02 nm in good agreement with the reticular distance of 0.203 nm of Ni(111), indicating that the steps are monoatomic. Islands of monoatomic height and depth are also observed. Their presence is assigned to the insufficient mobility of the Ni metal atoms to thoroughly anneal the reduced surface and completely heal out the structural modifications induced by the growth of the air-formed native oxide and its subsequent reduction.

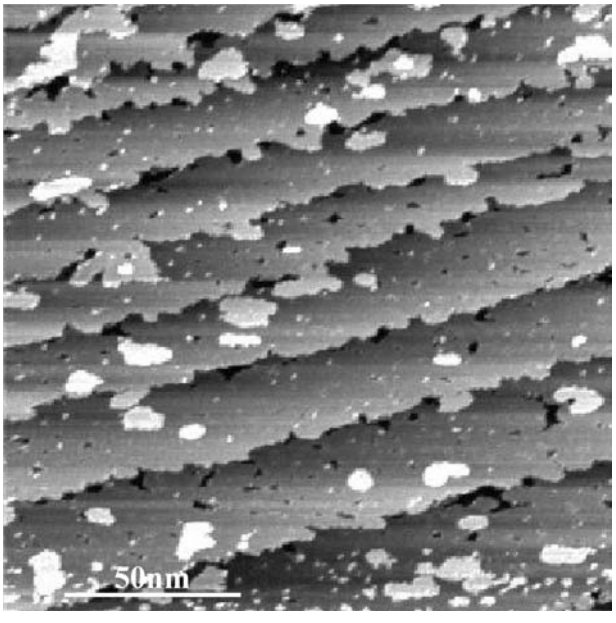

Fig. 2 Topographic EC-STM image of the Ni(111) surface recorded at $E = -1{,}150$ mV in 1 mM NaOH(aq) after cathodic reduction of the air-formed oxide ($I_{tip} = 0.5$ nA; $E_{tip} = -750$ mV; z range = 0.6 nm)

Figure 3 shows the topographic modifications generated by a potential step to −800 mV at the beginning of the A_1 anodic wave. A slow dissolution of the surface essentially localized at the step edges is observed. The resulting retraction of the step edges leads to the consumption of the terraces by a step flow mechanism. The dissolution starts right after the potential step from −850 mV to −800 mV and continues with time. Two arrows (marked D) are drawn in Fig. 3 to point to two sites where the terraces dissolve. It can also be seen that the islands of monoatomic height are consumed by the preferential dissolution at their edges, leading first to shrinking (Fig. 3b, c) and then to vanishing (Fig. 3d). A similar 2D mechanism has been observed in acid solution [12, 29] and is characteristic for the dissolution of surfaces polarized at small overpotential values. Soluble species, such as $HNiO_2^-$ or $NiOH^+$ have been assumed to be involved in the dissolution mechanism of nickel [20, 39–41]. Their formation cannot be discussed on the basis of our STM results, which do not provide chemical identification of the dissolving species.

In the image shown in Fig. 3b recorded from 30 s to 73 s after the potential step, some extended areas of lower apparent height (marked A in the image) are developed on the terraces. The height difference between these darker areas and the surrounding terrace areas is approximately 0.05 nm. These areas possibly correspond to islands of adsorbed OH^- species on the terraces of the Ni(111) surface that would take place at potentials less anodic than the one required to nucleate the passivating oxide on the terraces (see below). The formation of such islands of lower apparent height has previously been observed on Cu(111) and Cu(001) in 0.1 M NaOH(aq) at potentials below the oxide formation and corresponds to the adsorption of hydroxide [42–45]. The darker appearance on the terraces observed on Ni and Cu is assigned to an electronic effect commonly observed by STM for O species adsorbed on metal surfaces [46] and does not correspond to the true topography of the Ni surface possibly covered by the adsorbed OH^- species. It can be seen in Fig. 3c and d that these darker areas extend slightly but do not reach full coverage of the surface during the time scale of the measurement. No specific ordered superstructure is associated with the development of these islands on Ni, in contrast with Cu.

In the image shown in Fig. 3c, the step edges become decorated by grains (marked G) having a lateral size of 1.9 nm and appearing slightly higher than the step edges (0.07 nm). In Fig. 3d, some grains are isolated from the nearby dissolving step edges. These grains are assigned to nuclei of the passivating oxide. At this potential, the nucleation occurs preferentially at the step edges where it slows down or blocks the dissolution locally. The continuous faster dissolution of the step edges on the nearby sites not yet passivated isolates the passivated site from the dissolving terrace thus forming passivated

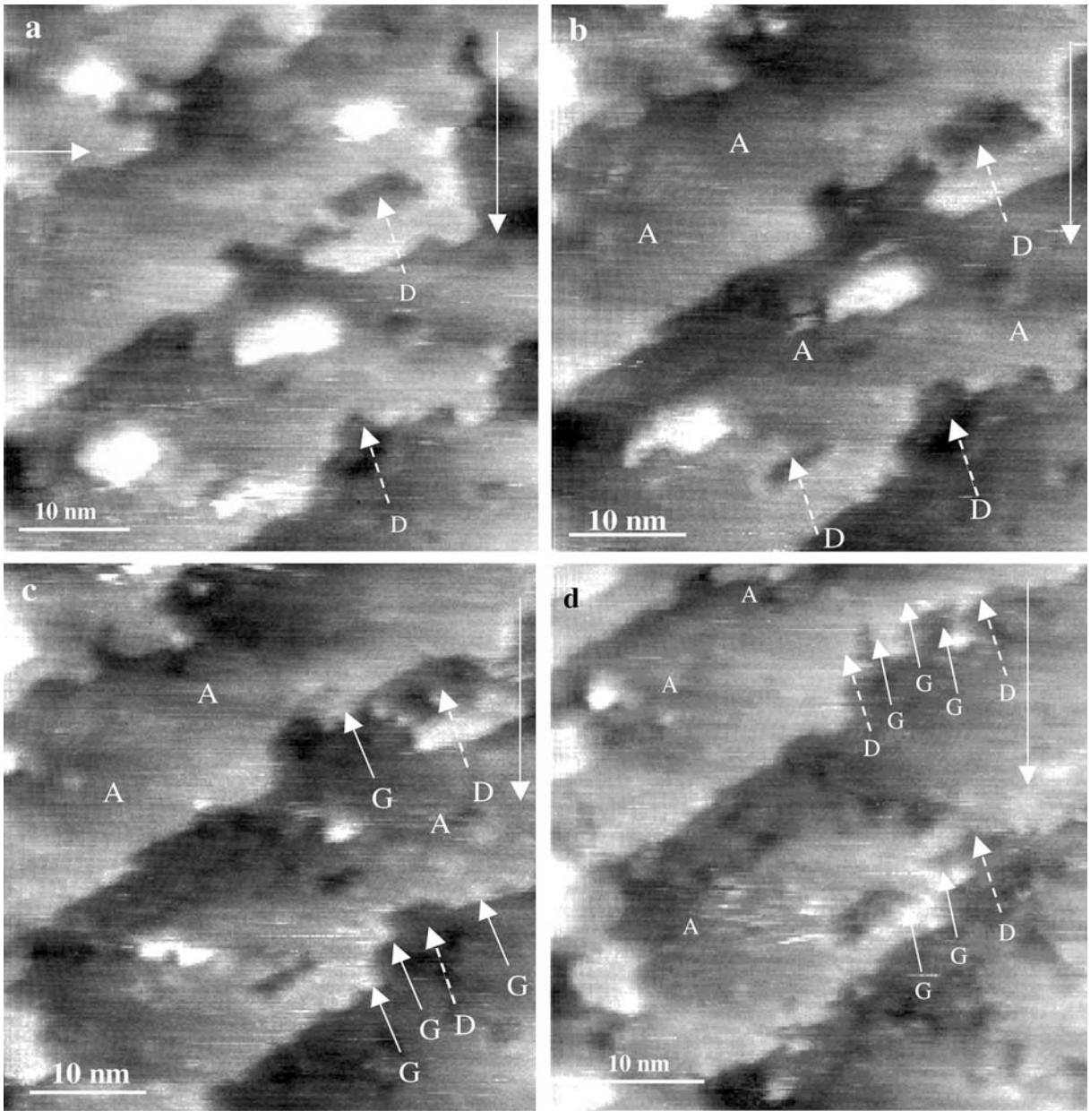

Fig. 3 Sequence of topographic EC-STM images (43 s/image) of the Ni(111) surface recorded in 1 mM NaOH(aq) ($I_{tip} = 0.7$ nA, $E_{tip} = -855$ mV, z range = 0.35 nm). **a** It was recorded while stepping the potential from $E = -850$ mV to -800 mV. The *horizontal arrow* marks the potential step. **b** Recorded between 30 s and 73 s after the potential step. **c** Recorded between 73 s and 116 s after the potential step. **d** Recorded from 164 s to 207 s after the potential step. The *vertical arrows* indicate the scan direction

and isolated islands. A similar process of roughening of the step edges has been previously observed for Cu(111) in a borate buffer aqueous solution and assigned to the nucleation of the passive layer [47]. Thus for Ni(111) in 1 mM NaOH (aq), the dissolution of the metallic surface and nucleation of the passivating oxide film are observed at -800 mV. However, at this potential, the growth of the passive film is slow and dissolution is the predominating process modifying the surface morphology.

Figure 4 shows the topographic modifications observed after stepping the potential from -960 mV to the more anodic value of -780 mV. Prior to the formation of the passive film, the dissolution of the Ni(111) surface is observed (some sites are marked D in Fig. 4b). Like at -800 mV, it is essentially localized at the step edges and leads to a step flow consuming the metallic terraces. The monoatomic pits and the depressions initially present in the terraces are enlarged by this mechanism. The fuzzy aspect of the image suggests a high surface mobility of the dissolving species. In Fig. 4c, the dissolution appears to be considerably slow down and even stopped at some sites, in agreement with the clearer aspect of the image indicative of much less surface mobility. This slower dissolution is assigned to the nucleation of the passivating oxide. The time resolution of the measurement and the fuzzy aspect of the image in Fig. 4b do not

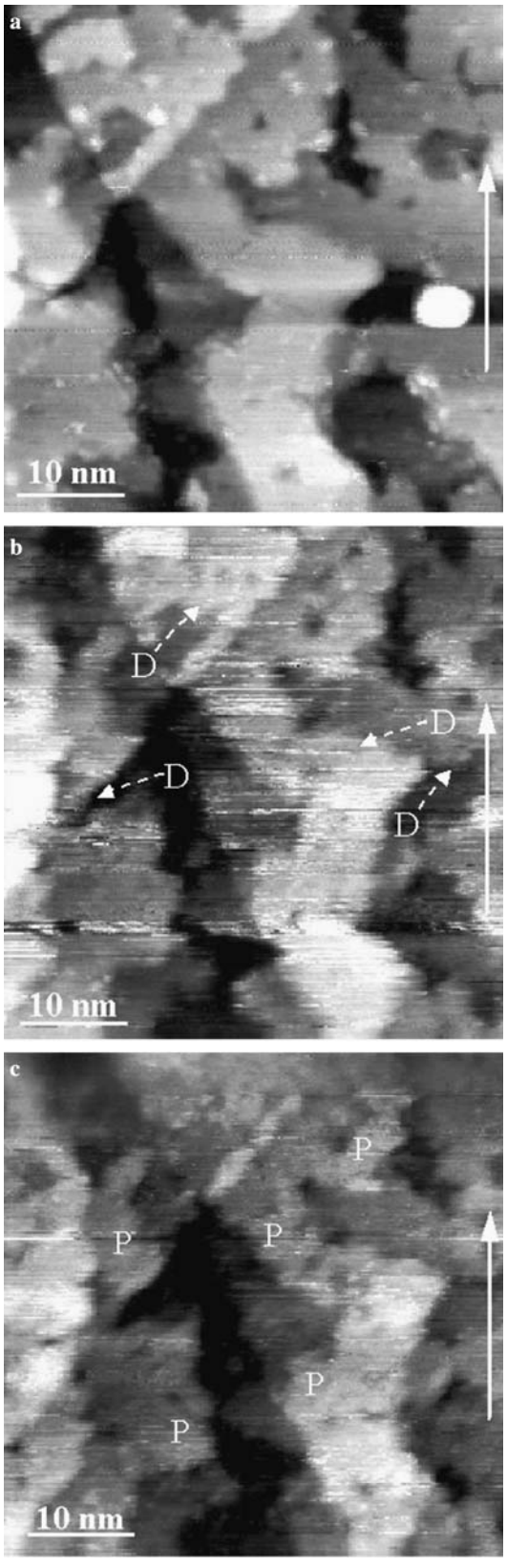

◀

Fig. 4 Sequence of topographic EC-STM images (100 s/image) of the Ni(111) surface recorded in 1 mM NaOH(aq) ($I_{tip}=0.5$ nA, $E_{tip}=-810$ mV in (**a**) and -930 mV in (**b, c**), z range = 0.9 nm in (**a**), 1 nm in (**b**) and 0.85 nm in (**c**). **a** Recorded at $E=-960$ mV, **b** and **c** were recorded 75 and 175 s after stepping the potential to $E=-780$ mV, respectively. The scan direction is indicated by the *vertical arrows*

allow the identification of oxide grains observed at -800 mV. However, protruding islands can be identified in Fig. 4c that are preferentially formed at and near the step edges (marked P). They are assigned to 2D islands formed by the nuclei of the passivating oxide. They nearly cover all the surfaces in Fig. 4c. This image shows the more advanced 2D growth of the passivating oxide after 175 s of polarization at this higher anodic potential.

The growth of the passive layer is confirmed by the image shown in Fig. 5a and b, recorded 775 s after the potential step at -780 mV and by the subsequent cathodic reduction experiments where a C_1 peak can be observed (see Fig. 5c). At this stage, the surface, showing a granular aspect, is completely covered by oxide islands. The lateral size of the individual grains ranges between 2 nm and 3 nm. Some of the substrate terraces can still be identified (as marked in Fig. 5), which is an indication that the passivating oxide is still 2-D. The resolution of the individual grains varies in the image, suggesting various degrees of coalescence of the grains. Locally, some grains present a nearly triangular morphology that is commonly observed at higher potentials (see below). This is a first indication of a crystallization process. The images obtained at atomic resolution after a more prolonged polarization (40 min after the potential step at -780 mV) confirm the presence of crystalline islands. The height difference between the crystalline islands and the noncrystalline areas in between is very low ($\sim$0.04 nm), indicating that the Ni(111) surface is completely covered by the crystalline nanograins at this stage. The measured lattice is hexagonal with a parameter of 0.306 ± 0.004 nm. This is consistent with the period of NiO(111) (0.295 nm), α-Ni(OH)$_2$(0001) (0.308 nm) or β-Ni(OH)$_2$(0001) (0.317 nm). A similar mechanism of passivation with 2D oxide islands covering first partially the metal surface has been observed for Cu in alkaline solution [48].

Figure 6 shows the topography observed after stepping the potential further anodically to -630 mV. The complete crystallization of the passive film is observed at this potential. It is characterized by the progressive development of a facetted topography not observed prior to the increase of potential and indicative of the full crystallization of the passive film. The facets have nearly the triangular morphology characteristic of the passive film formed on Ni [30–32, 35, 36]. The substrate terraces can no longer be identified in contrast with the image in Fig. 5. This is assigned to the further growth (i.e. thickening) of the crystalline passive film to form a 3D layer, in good agreement with previous studies concluding to the formation of a 3D passive film [7, 8, 11, 25]. At atomic resolution, a hexagonal structure is measured on the facets (see Fig. 5b). The lattice period is 0.318 ± 0.012 nm, slightly larger than that measured at

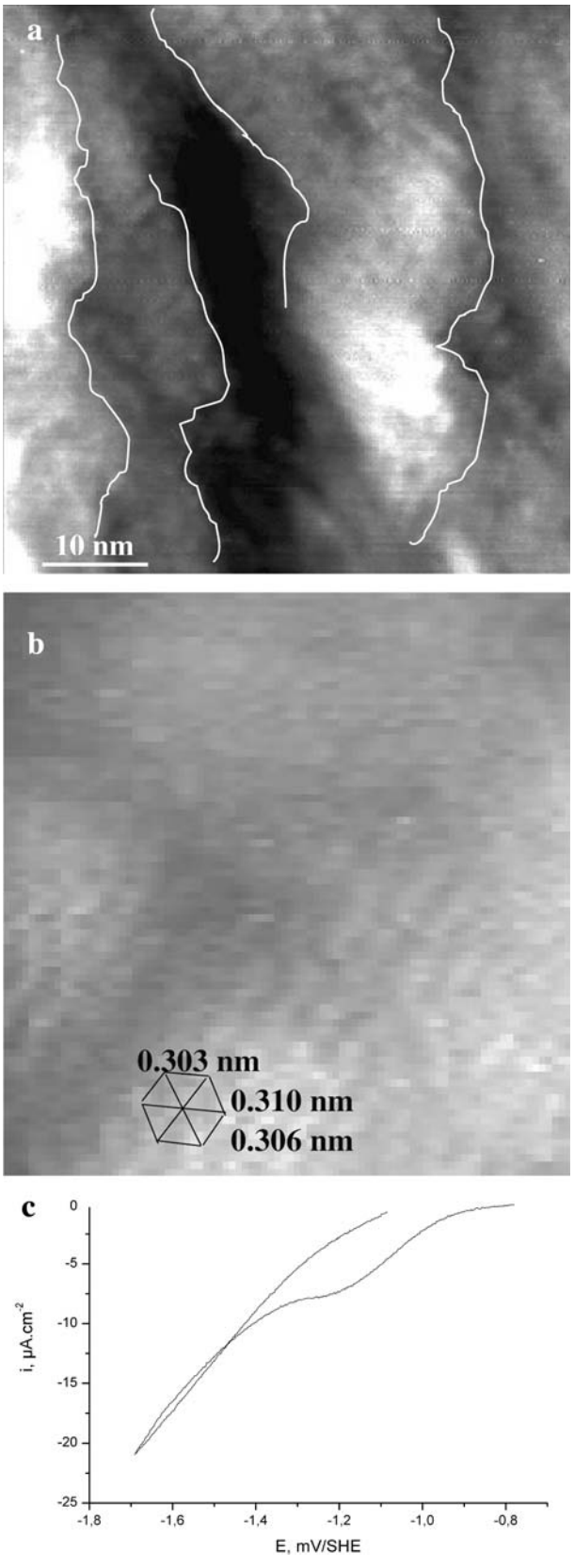

Fig. 5 Topographic EC-STM images of the Ni(111) surface recorded in 1 mM NaOH(aq) after stepping the potential from −960 mV to −780 mV. **a** $I_{tip} = 0.5$ nA, $E_{tip} = -930$ mV, z range = 0.70 nm. **b** $I_{tip} = 1.4$ nA, $E_{tip} = -930$ mV, z range = 0.15 nm) , **c** cathodic polarization curve of the oxide formed at −780 mV

−780 mV, and fitting better the lattice parameter of $Ni(OH)_2(0001)$ than that of NiO(111) (the assignment to α- or β-$Ni(OH)_2$ is discussed further on). The formation of facets is indicative of the tilt of the passive film lattice with respect to the substrate lattice as previously observed in acid solution [12, 30–32, 35–37]. This tilt can be associated with the transition to the growth of a 3D passivating oxide. It is to be noted that the C_1 peak was not observed in the cathodic reduction experiment performed after this series of STM measurements, despite a polarization at less anodic values than the critical value of −500 mV usually reported for the non reducibility of the Ni^{2+} layer and confirmed in our cyclic voltammograms. This is assigned to the effect of aging under polarization of the passive film (56 min at −780 mV followed by 51 min at −630 mV). Ageing at the relatively low potential also favors the growth of the 3D film, not observed in cyclic voltammetry measurements [7, 8, 11].

Figure 7 shows the topography of the passivated surface formed at −280 mV. At this high anodic potential in the passive range, the topography is also faceted. The terraces forming the facets have a width ranging from 3 nm to 5 nm. Many have a nearly triangular morphology pointing in the same direction and are better resolved in the lower part of the image. Their formation is also indicative of the tilt of the passive film lattice with respect to the substrate lattice. The atomic structure obtained on the facets has an hexagonal lattice with a parameter of 0.318 ± 0.015 nm (see Fig. 7b), in better agreement with the structure of $Ni(OH)_2(0001)$ (α or β) than with that of NiO(111). The larger parameter already measured at −630 mV when a 3D passivating oxide is formed is thus confirmed at −280 mV. Subsequent cathodic reduction experiments do not show the cathodic peak C_1 corresponding to the reduction of the Ni^{2+} oxide film. The surface topography remains facetted. The measurements are consistent with the polarization curves shown in Fig. 1 and confirm the nonreducible character of the 3D crystalline passive film formed at high anodic potential.

Discussion

Specific adsorption of hydroxide species

The STM observations performed at −800 mV at the onset of the anodic A_1 peak have revealed the formation of islands of lower apparent height (0.05 nm) on the terraces of the metal surface. This STM observation is similar to those recently reported for Cu(111), Cu(100) and Ag(111) in 0.1 M NaOH(aq) and suggest the adsorption of hydroxide species in a potential region negative to the formation of the oxide/hydroxide pas-

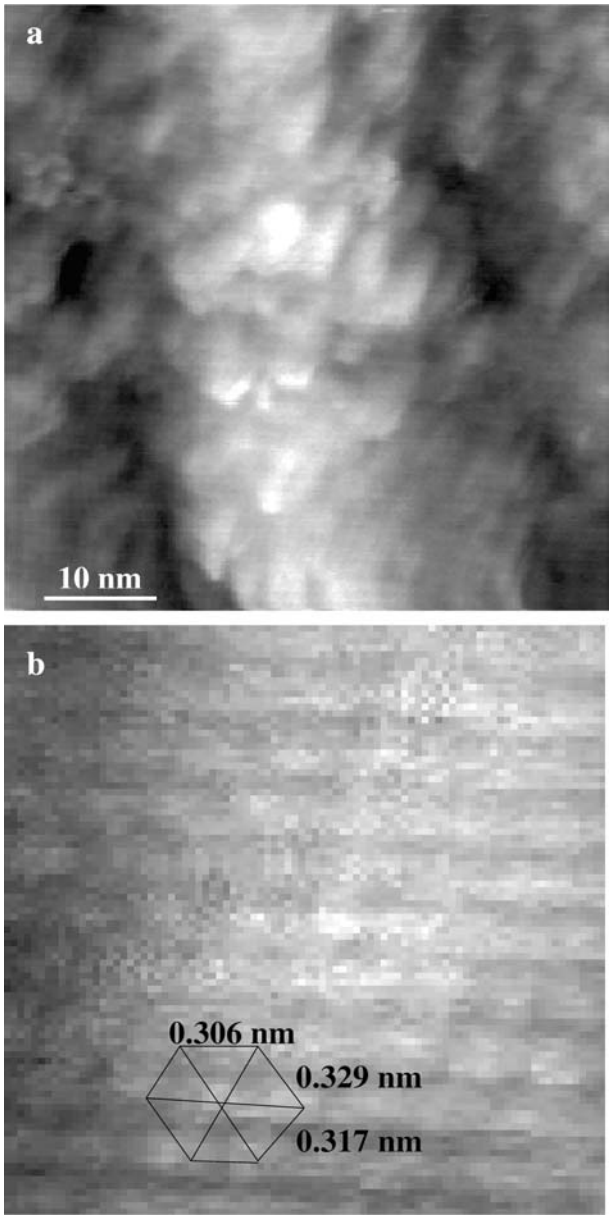

Fig. 6 Topographic EC-STM images of the Ni(111) surface recorded in 1 mM NaOH(aq) after stepping the potential to $E = -630$ mV ($I_{tip} = 1.3$ nA, $E_{tip} = -785$ mV, z range = 0.53 nm in (**a**) and 0.13 nm in (**b**))

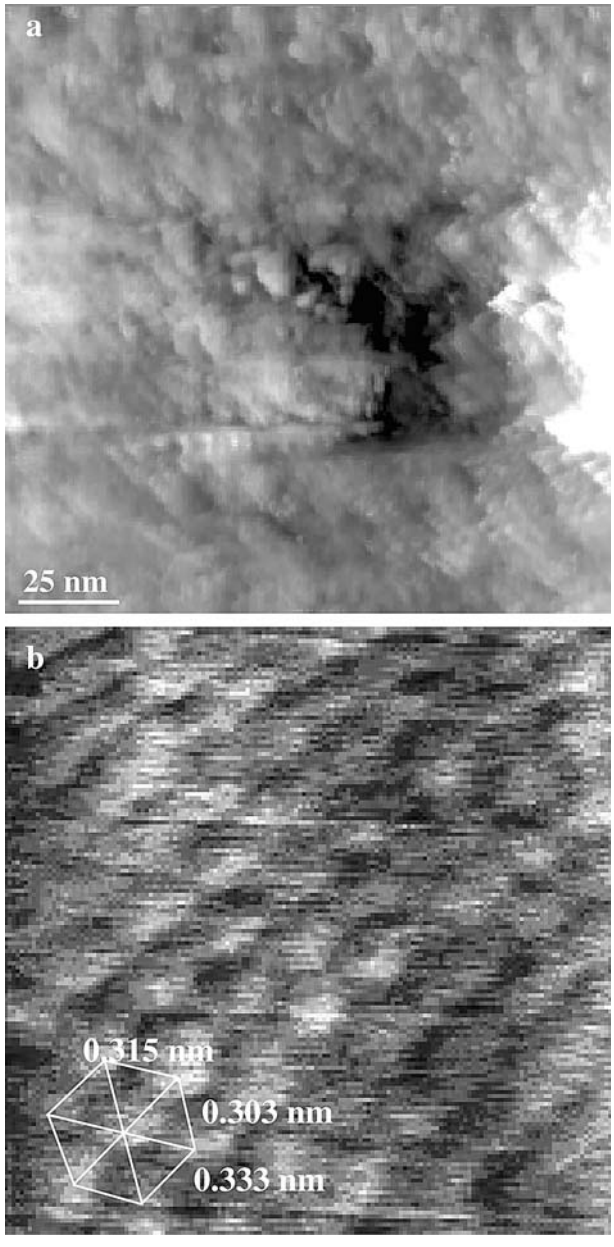

Fig. 7 Topographic EC-STM images of Ni(111) recorded in 1 mM NaOH(aq) at $E = -280$ mV ($I_{tip} = 1.2$ nA, $E_{tip} = -760$ mV, z range = 1.1 nm in (**a**) and 0.1 nm in (**b**))

sivating surface layer. On Cu [42–45], the adsorption and desorption of the OH^- species gives well-resolved anodic and cathodic peaks in the cyclic voltammetry measurements. Assuming a one electron discharge reaction of adsorption ($OH^- \Longleftrightarrow OH_{ads} + 1\ e^-$), the measured charge transfer corresponds to a surface coverage that is confirmed by the well-ordered superstructure formed by the OH_{ads} species and observed by EC-STM. These recent structural studies confirm the underpotential adsorption of hydroxide previously reported on this substrate [49–54]. On Ag, the adsorption of hydroxide at potential below the oxidation potential has also been reported [55–60]. The absence of specific anodic peaks in the cyclic voltammetry measurements led to the conclusion of a specific adsorption of OH^- species. This is associated with a marked modification of the surface structure of the metallic surface with lowering of the apparent height in the adsorbed islands [61] and formation of an ordered superstructure [62].

On Ni, there is no direct evidence of the adsorption of hydroxide species in the potential region negative to the formation of oxide/hydroxide compounds. However, the presence of adsorbed hydroxyl species, OH_{ads}, in the potential region below the A_1 peak has been proposed to explain the observed pH dependence of the electrooxidation of hydrogen on this substrate [10]. Also, theo-

retical calculation predicts that the adsorption of OH groups in the threefold hollow sites, the twofold bridge sites and the atop sites of the Ni(111) surface is exothermic [63]. The cyclic voltammograms obtained in the present study on Ni in 1 mM NaOH(aq) do not show any specific anodic and cathodic peaks that could be related to the adsorption and desorption of hydroxide ions accompanied by a charge transfer. This is an indication that the modifications of apparent height measured on the Ni(111) terraces could correspond to the specific adsorption of hydroxide not forming an ordered-superstructure on Ni(111). The absence of a well-ordered superstructure may be related to a weaker bonding and a higher mobility of the adsorbed hydroxide on Ni.

Nucleation and 2D growth of the passive film

The STM observations performed at −800 and −780 mV reveal that both the dissolution of the metal surface and the formation of oxide (or hydroxide) nuclei modify the surface topography in the initial stages of growth of the passive film. Both processes take place preferentially at the defects (i.e. terrace edges) of the metallic surface, leading respectively to step flow and to the roughening of the step edges by formation of the 2D grains of nanometer size (∼2 nm). The step flow generated by the preferential localization of the dissolution at the step edges has previously been observed at low overpotentials in acid solutions for Ni [12] and Cu [64] single-crystal surfaces and the roughening of the step edges related to the nucleation of the passive film have been previously observed for Cu in slightly alkaline aqueous solutions [45].

The results obtained in the present study show that the effect of the potential on the initial stages of 2D growth of the passivating oxide. At −800 mV, the nanograins, assigned to hydroxide (see below), nucleate at the step edges and can be isolated from the dissolving terrace due to the ongoing dissolution of the neighboring sites of the step edges not yet passivated. At slightly higher overpotential (−780 mV), hydroxide nanograins are also observed in the upper terraces in the vicinity of the passivated step edges and form extended islands of 2D nanograins thus increasing the surface coverage. The higher driving force for dissolution leads to a faster modification of the terraces and to the formation of indents in the terraces that can lead to 2D pits separating the islands of hydroxide nanograins.

In acid solution, the simultaneous dissolution of the Ni(111) surface and nucleation of the passive film have also been observed with EC-STM [32]. However, dissolution is considerably enhanced at low pH and leads to 3D roughening of the surface by creating 3D pits in the sites not yet passivated between the oxide grains. The results obtained here in alkaline solution show only a 2D roughening extending over the surface with time and are consistent with the formation of a 2D film consisting of hydroxide nanograins. These results provide a direct observation of a 2D growth mechanism previously deduced from CV measurements performed at low temperature (−90 °C) [11]. This growth mechanism characterized by nucleation at preferential sites followed by the lateral growth of islands of hydroxide nanograins is consistent with a solid state mechanism where the oxide formation result from the reaction of surface metal atoms with the solution species. A precipitation mechanism involving the deposition of corrosion products dissolved in the solution is not consistent with the very slow metal dissolution observed in these experiments.

3D growth and crystallization of the passive film

The results obtained in this study for $E \geq -780$ mV in 1 mM NaOH(aq) confirm the crystalline character of the passive film formed on nickel in aqueous solution as previously reported for passive films formed in acid [12, 30–33, 35–37] and alkaline [16, 38] electrolytes. In all the cases, a facetted topography of the passivated surface is observed in acid solutions [8, 10, 17–20, 22–32]. The facets have an hexagonal atomic structure that was assigned to NiO(111) stabilized by surface hydroxylation.

The present results obtained in alkaline solution show that an hexagonal atomic lattice with a small but significant increase of the lattice parameter from 0.306 nm to 0.318 nm with the transition from a mostly 2D film at −780 mV to a 3D film at $E \geq -630$ mV. The higher value measured when the film is 3D is in better agreement with $Ni(OH)_2(0001)$ (α or β) than with NiO(111). It is assigned to a thicker and continuous hydroxide outer layer of the passive film formed in alkaline solution, in good agreement with the 3D thickness reported for the outer hydroxide part of the passivating oxide formed in the Ni^{2+} passivation range [7, 8, 11, 20, 25]. The discrimination between the α or β forms of nickel hydroxide is delicate on the basis of the STM data alone. Nevertheless, the α form has been reported to be unstable in alkaline solution [65]. Moreover, it is described as semi-crystalline because of the possible H_2O intercalation between the hexagonal basal planes. As a consequence, the well-crystallized structure ($E \geq -630$ mV) is assigned to the stable β-$Ni(OH)_2(0001)$ structure. This is in good agreement with its nonreducible character, confirmed in our measurements and previously assigned to the formation of the β-$Ni(OH)_2$ phase [8, 9, 16].

At $E = -780$ mV, the passive film consists of nanocrystals having an hexagonal lattice with a smaller parameter of 0.306 nm. Since it is 2D, the distinction between the α or β form is meaningless (it must be viewed as a single monolayer of $Ni(OH)_2(0001)$ with no possible intercalation of water molecules that requires a multilayer film). Its structure can differ slightly from that of the 3D compound since the epitaxy with the substrate having the same hexagonal in-plane symmetry but a lower lattice parameter is expected to strain the lattice of the 2D overlayer, as previously observed on Ni(100) [38].

On Ni(111), assuming the formation of a (0001)-oriented monolayer of $Ni(OH)_2$ having the structure of the β phase, the strained epitaxy would induce a contraction of 3.8% of the hydroxide lattice.

The formation of a monolayer of NiO(111) (0.295 nm) cannot be fully excluded on the basis of our STM data. However, the growth of the passive film results from the reaction of the Ni atoms with hydroxide or hydroxyl species, and the formation of NiO involves a dehydroxylation reaction observed in the inner layer of the duplex 3D films formed on nickel [17–20, 22–32]. On Cr [66, 67] and stainless steels [68, 69], this reaction has been observed to be promoted by the increase of the potential and by ageing under anodic polarization. The fact that the nanocrystals discussed here are 2D and observed at the lowest anodic overpotential of formation leads us to exclude the formation of NiO.

Tilt of the oxide lattice

The crystalline structure of the Ni(111) surface passivated at $E \geq -630$ mV shows the typical faceted topography that is indicative of the tilt of the hydroxide lattice (and presumably of the inner oxide lattice of the film) with respect to the substrate lattice. This confirms, for a passive film consisting of a 3D inner layer of NiO and a 3D outer layer of $Ni(OH)_2$, the previous observations performed in acid solutions, where the film is essentially a 3D layer of NiO [12, 30–32, 35–37]. One essential new result presented here is that the tilt is also observed for the thicker films formed in alkaline solution and that the tilted epitaxy is related to the 3D growth of the film since it is not observed when the film is 2D and consists of nanocrystals having a lateral size of 2–3 nm.

Different models can be envisaged to explain this tilt. A first model is based on the 3D roughening of the oxide/metal interface induced by the extensive dissolution occurring in the initial stages of growth of the passive film in acid solution [32]. In this model, the oxide atomic planes are tilted because the oxide is growing above the succeeding steps of the substrate. This model might not be valid in our case since 3D roughening of the oxide/metal interface has not been observed in our experiments in alkaline solution where the dissolution is minimized.

A second model is based on the lowering of the interfacial energy by an improved match between the oxide (or hydroxide) and metal lattices [36]. The high density of boundaries between the 2D nanocrystals of the film provides multiple sites of possible relaxation of the stress induced by the lattice mismatch between the hydroxide nanocrystals and the metal substrate. In contrast, when the film is 3D, larger nanocrystals are expected to form by coalescence in the inner oxide layer of the passive film and the lower density of boundaries between the nanocrystals might not be sufficient for the relaxation of the stress induced by the lattice mismatch. This could induce the tilt between the lattices of the overlayer and substrate, contributing to the lowering of the interfacial energy (the lattice mismatch decreases with increasing tilt).

A third model is based on the mechanism of 3D growth of the oxide (or hydroxide) [70]. The tilted epitaxy implies the presence of misorientation dislocations at the oxide/metal interface. In the case of oxide growth by anion/vacancy diffusion control, anions can add to the misorientation dislocations of the oxide lattice to grow the oxide at the oxide/metal interface. In the case of oxide growth by cation/vacancy diffusion control, misorientation dislocations and misfit dislocations in the metal act as sources for cations. Cations diffuse to the external interface where the step edges correspond to the sites of growth of the oxide. Thus, the mechanism of 3D growth of the passive film, whether it proceeds by anion and/or cation diffusion control, produces interfacial misorientation dislocations that could also be the cause of the tilted epitaxy between the oxide lattice and the metal lattice.

Conclusion

The EC-STM measurements have been performed to study in situ the structural modifications of a single-crystal Ni(111) surface associated with the growth of the passivating Ni(II) oxide under controlled anodic polarization in 1 mM NaOH(aq).

At $E = -800$ mV, i.e. at the onset of the A_1 anodic peak corresponding to the growth of the passivating oxide, a slow dissolution of the nickel surface is observed. The dissolution takes place at the step edges, leading to the consumption of the metal terraces by a step flow mechanism. Islands of lower apparent height have been observed on the terraces that possibly correspond to the specific adsorption of hydroxide anions without formation of a specific superstructure. The nucleation of the passivating oxide occurs preferentially at the step edges at this potential. It is characterized by the formation of 2D grains with a lateral size of $\sim$2 nm. The ongoing dissolution at the nearby step edges not yet passivated leads to the formation of isolated 2D islands of the passivating oxide.

At $E = -780$ mV, dissolution of the metal terraces by step flow is still observed but the 2D growth of the passivating oxide is faster. It forms extended islands of 2D nanograins blocking the dissolution at the step edges. These 2D islands extend laterally with time to completely cover the surface. This leads to the formation of a 2D passivating oxide with a nanogranular morphology. The crystalline areas have a hexagonal lattice with a parameter of 0.306 ± 0.004 nm assigned to 2D nanocrystals of $Ni(OH)_2(0001)$ in strained epitaxy on Ni(111).

At $E \geq -630$ mV, the 3D growth of the passive film is observed. It is characterized by the formation of a facetted topography indicative of the tilt between the oxide lattice of the passive film and the lattice of the substrate.

The hexagonal lattice observed at atomic resolution at −630 and −280 mV has a parameter of 0.318 nm, slightly larger than that of 0.306 nm measured at −780 mV when a 2D passivating oxide is formed. The parameter is in excellent agreement with the value of 0.317 nm expected for an unstrained 3D layer assigned to β-$Ni(OH)_2(0001)$. This is consistent with the formation of a 3D outer hydroxide layer of the passive film formed in alkaline electrolytes, as opposed to the 2D outer hydroxide layer formed in acid electrolytes.

The nonreducibility of the passive film has been observed for $E \geq -500$ mV in potentiodynamic measurements and for $E \geq -630$ mV in potentiostatic measurements, showing a cathodic shift of the potential of nonreducibility with ageing of the passive film. It is consistent with the formation of a crystalline 3D layer of β-$Ni(OH)_2$ in the outer layer of the passive film.

References

1. Weininger JL, Breiter MW (1963) J Electrochem Soc 110:484
2. Mac Dougall B, Cohen M (1975) J Electrochem Soc 122:383
3. Mac Dougall B, Cohen M (1976) J Electrochem Soc 123:191
4. Mac Dougall B, Cohen M (1976) J Electrochem Soc 123:1783
5. Schrebler-Guzman RS, Vilche JR, Arvia AJ (1979) J Appl Electrochem 9:321
6. Burke LD, Twomey TAM (1984) J Electroanal Chem 162:101
7. Beden B, Floner D, Leger JM, Lamy C (1985) Surf Sci 162:822
8. Hahn F, Beden B, Croissant MJ, Lamy C (1986) Electrochim Acta 31:335
9. Beden B, Bewick A (1988) Electrochim Acta 33:1695
10. Floner D, Lamy C, Leger JM (1990) Surf Sci 234:87
11. Simpraga R, Conway BE (1990) J Electroanal Chem 280:341
12. Suzuki T, Yamada T, Itaya K (1996) J Phys Chem 100:8954
13. D'Alkaine CV, Santanna MA (1998) J Electroanal Chem 457:5
14. D'Alkaine CV, Santanna MA (1998) J Electroanal Chem 457:13
15. Grden M, Klimek K, Czerwinski A (2004) J Solid State Electrochem 8:390
16. Hirai N, Okada H, Hara S (2003) Transaction JIM 44:727
17. Dickinson T, Povey AF, Sherwood PMA (1977) J Chem Soc Faraday Trans I 73:327
18. Marcus P, Oudar J, Olefjord I (1979) J Microsc Spectrosc Electron 4:63
19. Hoppe H-W, Strehblow H-H (1980) Corrosion Sci 20:167
20. Paik WK, Szklarska-Smialowska Z (1980) Surf Sci 96:401
21. Lochel BP, Strehblow H-H (1984) J Electrochem Soc 131:713
22. Mitchell DF, Sproule GI, Graham MJ (1985) Appl Surf Sci 21:199
23. Delichere P, Hugot-Le Goff A, Yu N (1986) J Electrochem Soc 133:2106
24. Hummel RE, Smith RJ, Verink ED (1987) Corrosion Sci 27:803
25. Hoppe H-W, Strehblow H-H (1989) Surf Interface Anal 14:121
26. Biwer BM, Pellin MJ, Schauer MW, Gruen DM (1989) Surf Interface Anal 14:635
27. Wagner FT, Moylan TE (1989) J Electrochem Soc 136:2498
28. Hoppe H-W, Strehblow H-H (1990) Corros Sci 31:167
29. Marcus P (1991) In: Oudar J, Marcus P, Clavilier J (eds) Electrochemistry at well-defined surfaces. Special volume of J Chim Phys 88:1697
30. Zuili D, Maurice V, Marcus P (1997) In: Natishan P, Isaacs HS, Janik-Czachor M, Macagno VA, Marcus P, Seo M (eds) Passivity and its breakdown, PV 97-26. The Electrochemical Society Proceedings Series, Pennington, p 1013
31. Zuili D, Maurice V, Marcus P (2000) J Electrochem Soc 147:1393
32. Scherer J, Ocko BM, Magnussen OM (2003) Electrochim Acta 48:1169
33. Oudar J, Marcus P (1979) Appl Surf Sci 3:48
34. Cortes R, Froment M, Hugot-Legoff A, Joiret S (1990) Corros Sci 31:121
35. Maurice V, Talah H, Marcus P (1993) Surf Sci 284:L431
36. Maurice V, Talah H, Marcus P (1994) Surf Sci 304:98
37. Magnussen OM, Scherer J, Ocko BM, Behm RJ (2000) J Phys Chem B 104:1222
38. Yau S-L, Fan F-R F, Moffat TP, Bard AJ (1994) J Phys Chem 98:5493
39. Armstrong RD (1970) J Electroanal Chem 28:221
40. Sandoval R, Schrebler R, Gomez H (1986) J Electroanal Chem 210:287
41. Wronkowska AA (1993) J Electrochem Soc 140:995
42. Maurice V, Strehblow H-H, Marcus P (2000) Surf Sci 458:185
43. Kunze J, Maurice V, Klein LH, Strehblow H-H, Marcus P (2003) Electrochim Acta 48:1157
44. Kunze J, Maurice V, Klein LH, Strehblow H-H, Marcus P (2003) J Electroanal Chem 554(555):113
45. Maurice V, Strehblow H-H, Marcus P (2003) J Electrochem Soc 150:B316
46. Besenbacher F, Norskov JK (1993) Prog Surf Sci 44:5
47. Maurice V, Strehblow H-H, Marcus P (1999) J Electrochem Soc 146:524
48. Kunze J, Maurice V, Klein LH, Strehblow HH, Marcus P (2001) J Phys Chem B 105:4263
49. Ambrose J, Barradas RG, Shoesmith DW (1973) J Electroanal Chem 47:47
50. Droog JMM, Schlenter B (1980) J Electroanal Chem 112:387
51. Gennevo de Chiavo MR, Zerbino JO, Marchiano SL, Arvia AJ (1986) J Appl Electrochem 16:517
52. Härtinger S, Pettinger B, Doblhofer K (1995) J Electroanal Chem 397:335
53. Chan HYH, Takoudis CG, Weaver MJ (1999) J Phys Chem B 103:357
54. Marichev VA (2001) Surf Sci Rep 44:51
55. Droog JMM (1980) J Electroanal Chem 115:225
56. Lutzenkirchen-Hetch D, Strehblow H-H (1998) Electrochim Acta 43:2957
57. Iwasaki N, Sasaki Y, Nishina Y (1988) Surf Sci 198:524
58. Savinova ER, Kraft P, Pettinger B, Doblhofer K (1997) J Electroanal Chem 430:47
59. Zemlyanov DY, Savinova E, Scheybal A, Doblhofer K, Schlögl R (1998) Surf Sci 418:441
60. Jovic BM, Jovic VD, Stafford GR (1999) Electrochem Commun 1:247
61. Shaikhutdinov ShK, Savinova ER, Scheybal A, Doblhofer K, Schlögl R (2001) J Electroanal Chem 500:208
62. Kunze J, Strehblow H-H, Staikov G (2004) Electrochem Commun 6:132
63. Yang H, Whitten JL (1997) Surf Sci 370:136
64. Vogt MR, Lachenwitzer A, Magnussen OM, Behm RJ (1998) Surf Sci 399:49
65. Delahaye-Vidal A, Beaudoin B, Sac-Epée N, Tekaia-Elhsissen K, Audemer A, Figlarz M (1996) Sol State Ionics 84:239
66. Maurice V, Yang W, Marcus P (1994) J Electrochem Soc 141:3016
67. Zuili D, Maurice V, Marcus P (1999) J Phys Chem B 103:7896
68. Maurice V, Yang W, Marcus P (1996) J Electrochem Soc 143:1182
69. Maurice V, Yang W, Marcus P (1998) J Electrochem Soc 145:909
70. Hirth JP, Pieraggi B, Rapp RA (1995) Acta Metall Mater 43:1065